Available online at www.sciencedirect.com
SCIENCE DIRECT
Surface Science 600 (2006) 2079–2090
SURFACE SCIENCE
www.elsevier.com/locate/susc

Comparison of S, Pt, and Hf adsorption on NiAl(1 1 0)

Karin M. Carling [a], Will Glover [b], Hakan Gunaydin [b], Tracy A. Mitchell [b], Emily A. Carter [a,b,*]

[a] Department of Mechanical and Aerospace Engineering and Program in Applied and Computational Mathematics, Princeton University, Princeton, NJ 08544-5263, United States
[b] Department of Chemistry and Biochemistry, University of California, Los Angeles, CA 90095-1569, United States

Received 13 August 2005; accepted for publication 23 February 2006
Available online 27 March 2006

Abstract

First-principles periodic slab density-functional theory (DFT) calculations with a plane-wave basis are used to predict the properties of S, Pt, and Hf adsorption on NiAl(1 1 0). Stable adsorption sites are identified, and adsorbate binding energies and structures are predicted. We find that while S adsorbs in a threefold site, the metals prefer to adsorb in the Ni–Ni twofold bridge site. The latter finding is consistent with scanning tunneling microscopy experiments for adsorption of various transition metals on NiAl(1 1 0) by Ho and coworkers. S is predicted to easily diffuse between threefold sites. We find that Pt and Hf both induce significant changes in the local surface structure, changing twofold bridge sites into fourfold coordination sites by drawing next-nearest-neighbor atoms nearly equidistant with the nearest-neighbor atoms. We find Pt favors interaction with Al slightly more than Ni, while Hf shows a particularly strong affinity for Ni compared to Al. We also predict that Hf may diffuse one-dimensionally along Ni rows with a barrier of ≈0.6 eV.

Keywords: NiAl alloy; (1 1 0) surface; Adsorption; Hf; Pt; S; DFT

1. Introduction

NiAl alloys are industrially important lightweight materials used in bimetallic catalysts [1] and in high temperature applications [2]. For the latter, their high melting points and excellent corrosion resistance [3] (below 1300 °C) make them particularly useful for engine applications, e.g., in thermal barrier coatings for jet turbine engines [4,5]. Ni-based superalloys, primarily composed of Ni_3Al in a Ni matrix, form the basis of metal components in such gas turbine engines. These engine components are protected by a multilayer thermal barrier coating (TBC) that includes a metallic bond coat. More specifically, typical bond coat alloys either contain primarily Ni, with Cr, Al, and Y dopants [6–8], or are based on NiAlPt alloys [9,10]. Other elements may be present in small quantities, either added purposefully as dopants (e.g., Hf) [9], or present as impurities that accumulate during the manufacturing process (e.g., S) [10]. These impurities and alloying elements are thought to affect the properties of the interface between the bond coat and the protective aluminum oxide layer that grows during operation of the jet engine.

The β-NiAl phase forms the basis of Ni–Al–Pt alloys used for TBC bond coats [10]. Its structure is the B2 or CsCl structure, which is a bcc lattice with one element at the corners and the other at the body center of the cubic unit cell. This phase has the highest melting point of all NiAl intermetallics (1638 °C) [11]. When Pt is added to β-NiAl, it preferentially substitutes at Ni sites [10]. The addition of Pt improves the properties of this alloy as a bond coat by somehow improving the alumina scale adhesion. The mechanism for this improvement is unclear. In

* Corresponding author. Address: Department of Mechanical and Aerospace Engineering and Program in Applied and Computational Mathematics, Princeton University, Princeton, NJ 08544-5263, United States. Tel.: +1 609 258 5391; fax: +1 609 258 5877.
E-mail address: eac@princeton.edu (E.A. Carter).

0039-6028/$ - see front matter © 2006 Elsevier B.V. All rights reserved.
doi:10.1016/j.susc.2006.02.047

the present work, we investigate adsorption of Pt on a NiAl surface, in order to take a first step toward understanding the interactions of Pt in the NiAl bond coat.

Of all possible low-index surfaces of NiAl, the (1 1 0) surface is the closest packed. It is also stoichiometric, with equal amounts of Ni and Al organized in alternating rows [12]. It is predicted to be the most stable of the low-index NiAl surfaces, according to density functional theory (DFT), within the local density approximation (LDA) and the full-potential linearized augmented plane-wave (FLAPW) method [13]. This surface has attracted considerable interest, ever since the first low-energy electron diffraction (LEED) [14] and medium energy ion scattering (MEIS) [15] experiments suggested a rippled surface structure. The surface relaxes from its truncated bulk structure to a rippled surface in which the Al rows rise out from the surface and the Ni rows contract toward the bulk. Kang and Mele [16] proposed that this relaxation is driven by a smoothing of the surface charge density. If the Al atoms relax outward, they asserted that the kinetic energy of the sp electrons will be reduced. The resulting charge density will push the Ni atoms inward toward the bulk. The rippling can also be viewed as a preference for the larger atom and the element exhibiting lowest surface energy to move toward vacuum. The radius of Al is 1.43 Å, 14% larger than the Ni atom (radius of 1.25 Å), suggesting that strain may be relieved by allowing the larger Al atom to move toward vacuum. Also, the surface energy of Al(1 1 1) is considerably smaller [17] than the surface energy of Ni(1 1 1) [18], and since the surface energy is the main contribution to the surface segregation energy [19], an impurity with a lower surface energy than the host is more likely to segregate to the surface. This segregation perspective also supports a rippling with Al atoms rising out of the surface.

The stability of the NiAl(1 1 0) surface has made it a model system for investigating the properties of ordered bimetallic surfaces; hence its properties have been studied extensively both experimentally [14,15,20–22,12,23,24] and theoretically [16,25,23]. Both measurements by angle-resolved photoemission and predictions by DFT-LDA pseudopotential calculations of the surface electronic structure agree that the surface is nonmagnetic, just as in bulk NiAl [23].

Moving beyond the clean surface, adsorption on NiAl(1 1 0) has been the topic of experiments and theory alike. For example, the interaction of hydrogen with NiAl(1 1 0) has been studied in order to better understand the catalytic properties of this surface [26,1,27–29]. According to a He atom scattering study [28], atomic hydrogen adsorbs in the Ni–Ni twofold bridge site. DFT calculations within both LDA and the generalized gradient approximation (GGA) predict H atoms to adsorb slightly off the Ni–Ni twofold bridge site [1,29]. It was postulated from DFT-GGA (non-self-consistent, based on a DFT-LDA charge density) calculations that the interaction of H_2 is stronger at Ni sites than at Al sites, due to mixing between the H_2 bonding and anti-bonding orbitals and the 3d-orbitals of Ni [26]. Variable temperature LEED experiments of H_2 dissociation on NiAl(1 1 0) concluded that the dissociation is an activated process [1], consistent with DFT-GGA predictions [30]. The heat of adsorption of atomic hydrogen on pure Ni(1 1 0) is larger than on pure Al(1 1 0) [31], consistent with the observed preference for Ni-dominated H adsorption sites on the NiAl(1 1 0) surface.

Adsorption of oxygen on NiAl(1 1 0) has been studied theoretically by finite-temperature DFT-LDA calculations, which predict that O atoms will adsorb in the Ni–2Al threefold site [32], with shorter O–Al than O–Ni bonds. Thus, oxygen has a preference for Al-dominated sites, in contrast to hydrogen which prefers Ni-dominated sites. Experimentally, the preference for Al–O interaction has been seen in a LEED and Auger electron spectroscopy (AES) study [33]. This is consistent with the larger heat of adsorption of O_2 on pure Al(1 1 1) compared with pure Ni(1 1 1) [34–37].

Lately, the NiAl(1 1 0) surface has been used as a substrate for single-molecule vibrational spectroscopy [38,39] and investigations of the properties of metallic dimers and chains by scanning tunneling microscopy (STM) [40,41]. All metal atoms are found to adsorb in the Ni–Ni bridge site, as in hydrogen atom adsorption.

Here we explore the adsorption of some TBC impurities and dopants on NiAl(1 1 0), as a model for the NiAl-based bond coat. We use DFT to investigate the clean NiAl(1 1 0) surface, as well as the adsorption of S, Pt, and Hf on this surface. These elements are known to segregate to solid–solid interfaces such as $NiAl/Al_2O_3$ [42]; knowledge about the adsorption properties of these elements at a free surface provides a reference point for understanding their behavior at related solid–solid interfaces. Additionally, characterization of Hf and Pt adsorption may also shed light on why metal atoms generally prefer to adsorb in the Ni–Ni bridge site. Section 2 provides details of the calculations. Results for the clean surface are presented in Section 3 and for S, Pt, and Hf adsorption in Sections 4.1, 4.2, and 4.3, respectively. Finally, our conclusions are given in Section 5.

2. Calculational details

We employed the VASP implementation [43–45] of spin-polarized DFT [46,47] with the Perdew–Burke–Ernzerhof (PBE) version [48] of the generalized gradient approximation (GGA) for electron exchange and correlation. The electron–nuclear interaction is described by projector augmented wave (PAW) potentials [49,50] for all elements; the PAW-DFT method is an all-electron DFT within the frozen core approximation. We used kinetic energy cutoffs of 400 eV for bulk NiAl, 300 eV for S/NiAl(1 1 0), 320 eV for Pt/NiAl(1 1 0), and 480 eV for Hf/NiAl(1 1 0), yielding total energies converged to at least 1 meV/atom for all systems. In fact, the total energy for bulk NiAl is converged at a kinetic energy cutoff of 300 eV, but these calculations at 400 eV cutoffs were performed to be consistent with other related research on $NiAl/Al_2O_3$ (to be published

elsewhere). The integration of the Brillouin zone was done with the Methfessel–Paxton Fermi surface smearing method [51], with a smearing width of 0.1 eV. PAW-DFT-GGA(PBE) theory, with a 400 eV kinetic energy cutoff and a $18\times18\times18$ Monkhorst–Pack k-point grid [51] (165 irreducible k-points) in the primitive 2-atom unit cell, yields a lattice parameter of 2.88 Å and a bulk modulus of 158 GPa for bulk NiAl, both of which are within 1% of experiment [52,1].

Several cell geometries were employed. The clean NiAl(1 1 0) surface was modeled using a cell with a minimum surface area, containing one Ni and one Al atom per layer, and a converged Γ-point-centered $17\times15\times1$ Monkhorst–Pack k-point grid (72 irreducible k-points), which produces total energies converged to <0.1 meV/atom. The adsorbate–substrate systems were mainly modeled with a cell containing one adatom, four Ni atoms, and four Al atoms per layer, i.e., a 2×2 supercell, corresponding to an adsorbate coverage of 0.125 monolayer (ML). One monolayer is defined as a layer with the same number of atoms as the top layer of the substrate, i.e., for our 2×2 cell 1 ML corresponds to 8 atoms. This cell was sampled in k-space by a converged grid of $9\times7\times1$ points (20 irreducible k-points). Increasing the grid to $11\times9\times1$ changed the total energy by less than 1 meV/atom. Lower adsorbate coverages (0.056 ML) were also explored within a 3×3 supercell, with nine Ni and nine Al atoms per layer, and a $7\times5\times1$ k-point grid (12 irreducible k-points). The k-point grid was chosen to give at least the same or better k-point sampling as for the two smaller surface unit cells. In this larger cell, we explored adsorption of Pt in the Ni–2Al threefold and Al–Al and Ni–Ni bridge sites, and of S in the 2Ni–Al threefold and Ni–Ni bridge sites, since the adsorption energies for these sites in the 2×2 cell are very similar and we wanted to further verify the energy ordering of the states. The adsorption energies at this lower coverage were found to be ≈0.1 eV larger than for the 2×2 supercell, but going to lower coverage did not change the energy ordering of the sites. Since the changes in the adsorption energies were small, we used the 2×2 supercell (0.125 ML) for the rest of our analysis. All NiAl(1 1 0) slabs were five layers thick, with at least 12 Å of vacuum in the surface normal direction. The five layer slab produced converged properties, as will be discussed in Section 3.

We used the conjugate gradient method, as implemented in VASP, to relax the ionic positions of the NiAl(1 1 0) slab and the adsorbates. The atoms of the top three layers of the slab were allowed to relax while the two bottom layers were kept fixed at their bulk positions, with the lateral lattice vectors fixed at the DFT-GGA equilibrium bulk value for NiAl. Adsorbates were initially positioned in each of the seven possible high-symmetry sites (see Fig. 1), with the initial coordinate normal to the surface derived from atomic radii. To reduce the computational time used, we first allowed only relaxation of the adsorbate in the surface normal direction before allowing full relaxation in all directions. We compared these results with immediate full relaxation in all directions, as well as starting with adsorbates on bulk truncated or relaxed clean surface structures, for representative systems. No significant differences between the results produced by various structural optimization strategies were found. Ionic positions were relaxed until the forces were less than 0.05 eV/Å. For some test cases, ionic positions were relaxed until forces were less than 0.01 eV/Å; again this did not produce any significant structural changes.

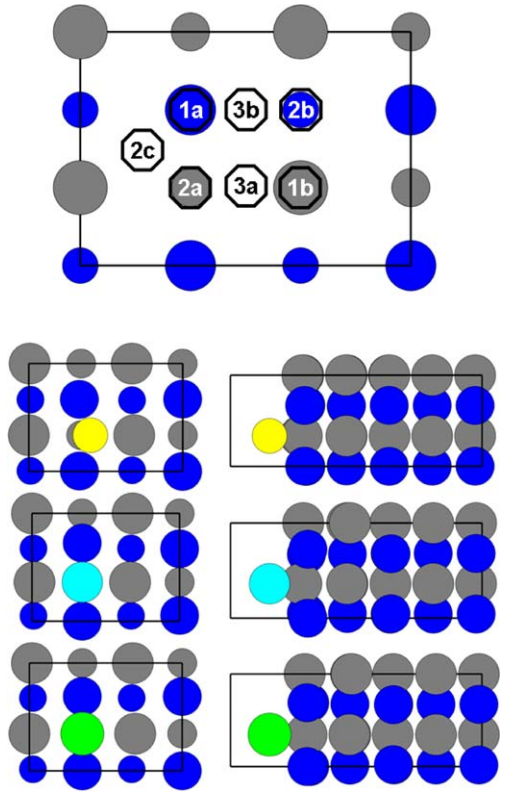

Fig. 1. The seven possible high-symmetry sites on the NiAl(1 1 0) surface (top) and the most stable adsorption sites (bottom) for the three adsorbates: S, Pt, and Hf. Blue circles represent the Ni atoms, gray circles represent the Al atoms, and the atoms with smaller radii are in the second layer. The hexagons symbolize the seven possible adsorption sites. Site 1a is the Ni on-top site, 1b the Al on-top site, 2a the Ni–Ni bridge site, 2b the Al–Al bridge site, 2c the Ni–Al bridge site, 3a the 2Ni–Al threefold site, and 3b the Ni–2Al threefold site. The six lower panels show the preferred adsorption sites for S (yellow, top), Pt (light blue, middle), and Hf (green, bottom), respectively. The panels on the left hand side show the top view, and the right hand side is the side view. (For interpretation of the references in colour in this figure legend, the reader is referred to the web version of this article.)

Adsorbate binding energies are reported relative to the structurally relaxed clean NiAl(1 1 0) surface and the ground state isolated atom, according to

$$E_{\mathrm{ads,X}} = E^{\mathrm{tot}}_{\mathrm{X/NiAl}} - (E^{\mathrm{tot}}_{\mathrm{X}} + E^{\mathrm{tot}}_{\mathrm{NiAl}}), \quad (1)$$

where $E^{\mathrm{tot}}_{\mathrm{X/NiAl}}$ is the total energy of the adsorbate–substrate system, $E^{\mathrm{tot}}_{\mathrm{X}}$ is the energy of the ground state isolated atom X, $E^{\mathrm{tot}}_{\mathrm{NiAl}}$ is the energy of the clean NiAl(1 1 0) surface slab, and X denotes the particular adatom, i.e., S, Pt, or Hf.

The calculations for the isolated atoms were performed in a $12 \times 12 \times 12$ Å cell for S and Pt, and a $14 \times 13 \times 12$ Å cell for Hf, with no k-point sampling. The kinetic energy cutoff for the plane-wave expansion was 480 eV for all elements, which gave a total energy convergence of 1 meV/atom or better for the isolated atoms. The resulting orbitals were analyzed to check that convergence to the appropriate electronic ground state was reached for each element: approximately ^3P (s^2p^4) for S, ^3D (s^1d^9) for Pt, and ^3F (s^2d^2) for Hf. Spin-contamination in spin-polarized DFT produces only approximate ground states.

The surface dipole corrections for the adsorbate–substrate systems were calculated a posteriori. For S and Pt adsorbate–substrate systems, the correction was less than 3 meV for the total energy of the cell. For Hf the correction was quite large; in Table 3 we report both uncorrected and corrected adsorption energies for Hf. The correction does not change the energy ordering of the states.

We analyzed the vibrational frequencies of the adsorbates to be able to distinguish between minima, transition states (TS), and higher order saddle points (HOSP). This is done by displacing the adsorbate, and all metal atoms within a 3 Å radius of the adsorbate, a short distance (±0.02 Å) in all three directions. These displacements produce forces on the atoms that are used to derive the force constant (Hessian) matrix from a finite difference construction. The eigenvalues of the Hessian matrix give the frequencies. For a minimum energy state, all frequencies are real, whereas a TS has one imaginary frequency, and a HOSP has two or more imaginary frequencies. If the magnitude of the imaginary frequency in a system with only one imaginary frequency was less than 50 cm^{-1}, we designate this adsorption site with "TS", since the frequency is too small to unambiguously assign it as a transition state.

Electron density differences, $\Delta\rho$, were calculated from the electron densities from all three systems (X/NiAl(1 1 0), NiAl(1 1 0), and X = S, Pt, Hf), all with the same cell size and computational parameters, i.e., the ones used for the adsorbate–substrate (X/NiAl(1 1 0)) calculations. Solely for the purposes of constructing $\Delta\rho$, the clean NiAl(1 1 0) density and isolated atom density are then calculated by removal of the adatom or the NiAl(1 1 0) substrate, respectively, from the adsorbate–substrate (X/NiAl(1 1 0)) structure such that the remaining atoms are in the same positions as in the adsorbate–substrate system.

We also analyzed the projected local density of states (LDOS) for the adsorbates and their nearest neighbors. This analysis strongly depends on the choice of radius for the Wigner-Seitz cell that sets the size of the local sphere in which the LDOS are analyzed. Ref. [53] provides a more detailed discussion on how to choose the radii. Here, we choose to use the atomic radii for the elements, i.e., a radius of 1.246 Å for Ni, 1.432 Å for Al, 1.025 Å for S, 1.388 Å for Pt, and 1.564 Å for Hf. The LDOS information is separated into spin-up and spin-down components and projected onto s, p, and d atomic orbitals. We caution that interpretation of these projections can only be trusted in a qualitative sense due to the numerical approximations employed.

3. Clean NiAl(1 1 0) surface

Table 1 displays surface energies, γ, for NiAl(1 1 0) slabs as a function of the number of atomic layers. The surface energy converges quickly with slab thickness to 1.57 J/m^2. This is lower than earlier DFT-LDA values that range from 1.79 to 2.85 J/m^2 [54], but larger than a previously reported DFT-GGA prediction of 1.37 J/m^2 [32]. The GGA results are expected to be more reliable, since surface energies involve the breaking of bonds, a process whose energy LDA is well known to overestimate. Experimentally, the surface energy was determined to be 1.4 J/m^2 for stoichiometric NiAl just above the melting temperature [2]. As expected, the GGA results are in fair agreement with the experimental estimate.

Table 1 also presents the intralayer structural relaxations, as characterized by the rippling of the first surface layer $\Delta d_{11} = z(\mathrm{Al}) - z(\mathrm{Ni})$, where z(X) is the z-coordinate of the X atom of the outermost layer of the clean NiAl(1 1 0) surface. These structural changes exhibit slower convergence with respect to the slab thickness than the surface energy. The thinnest slab used predicts a rippling of 0.18 Å, which is 10% greater than the rippling in the thickest slab considered. The slab with five layers of NiAl exhibits a structure and energy consistent with the thickest slab examined; we therefore used this slab thickness in the subsequent adsorption calculations.

The surface rippling is in fair agreement with earlier measurements and theoretical predictions (see Table 2). The measured changes in the two interlayer distances closest to the surface, d_{12} and d_{23} (where $d_{ij} = z_j - z_i$ and i and j are indices of the atomic planes and where the plane closest to the vacuum is designated as 1) have errors of ±1–2% experimentally. Our results agree qualitatively with the measurements but mostly lie outside the experimental range. Early DFT-LDA predictions show exaggerated rippling [16,25], probably because only the atoms of the first

Table 1
Convergence of clean NiAl(1 1 0) surface properties

System	γ (J/m^2)	Δd_{11} (Å)
3 layers + $7d_z$ vacuum	1.570	0.183
5 layers + $7d_z$ vacuum	1.569	0.165
7 layers + $7d_z$ vacuum	1.570	0.172
9 layers + $9d_z$ vacuum	1.565	0.166
DFT-GGA (BP88, LDA structure, 4 layers + $4d_z$ vacuum)[a]	1.37	0.20
Experiment	1.4[b]	0.20[c]

The size of the vacuum layer is given in integer multiples of NiAl(1 1 0) interplanar distances, $d_z = 2.06$ Å. The surface energy γ converges faster than the surface rippling Δd_{11}, which is converged for slabs with five or more layers.

[a] Ref. [32].
[b] Ref. [10].
[c] Refs. [14,15].

Table 2
Comparison of measured and predicted rippling, Δd_{11}, of the clean NiAl(1 1 0) surface

Method	d_{12} (%)		d_{23} (%)		Δd_{11} (Å)
	Ni	Al	Ni	Al	
This work (PAW-DFT-GGA(PBE))	−3.0	+3.0	−1.65	+1.0	0.17
Kang/Mele (PP-DFT-LDA)[a]	−6	+6	...	...	...
Lee/Fu/Freeman (FLAPW-DFT-LDA)[b]	−8.0	+1.5	...	...	0.20
Hammer/Scheffler (PP-DFT-LDA)[c]	−7.0	+4.5	...	...	0.23
Hammer et al. (USPP-DFT-GGA(PW91))[d]	−4.75	+3.78	−1.12	+0.39	0.17
Davis/Noonan (LEED)[e]	-4.6 ± 1	$+5.2 \pm 1$	$+1 \pm 1$–2	$+2 \pm 1$–2	0.199
Yalisove/Graham (MEIS)[f]	-7 ± 1	$+5 \pm 1$	$+1 \pm 2$	-1 ± 2	0.204

Changes in the interlayer distances, d_{12} and d_{23}, are reported in percent of the interlayer distance of the (1 1 0) planes in the perfect bulk crystal ($d_z = 2.046$ Å). Predicted and measured rippling and interplanar distances of the clean NiAl(1 1 0) surface.
[a] Ref. [16].
[b] Ref. [25].
[c] Ref. [1].
[d] Ref. [64].
[e] Ref. [14].
[f] Ref. [15].

layer of the NiAl slab were allowed to move. The rippling was derived by fitting a 2D function to the LDA energies of ≈10 structures. The finding that only relaxing the first layer produces a larger rippling is supported by our results for the three-layer slab, where only one layer of the slab was relaxed, and there we see an exaggerated rippling (see Table 1). More recent DFT calculations on this surface, where the surface rippling was determined by full ionic relaxation schemes, show that LDA slightly overestimates the rippling, while GGA underestimates it, as we find here.

4. Adsorption

The single element bcc(1 1 0) surface has four high-symmetry sites: threefold, long-bridge, short-bridge, and on-top. Small adsorbates (e.g., hydrogen [55–57]) on bcc(1 1 0) metal surfaces occupy the threefold adsorption site, since it gives the highest coordination for a small atom. Larger adsorbates, e.g., carbon [58] or sulfur [59,60], seem to prefer the long-bridge site that can give a large enough atom an essentially fourfold coordination.

The binary NiAl(1 1 0) surface is a bcc(1 1 0) surface with two components with seven high-symmetry sites as possible adsorption sites, as shown in Fig. 1. There are two sites with threefold coordination, with either two Ni and one Al (2Ni–Al) or one Ni and two Al (Ni–2Al), which produce different chemical environments for the two threefold sites. The two bridge sites from the single element (1 1 0) bcc surface give rise to three bridge sites on the NiAl(1 1 0) surface: one short-bridge site with one Ni and one Al atom (the Ni–Al bridge), and two long-bridge sites, one with Ni atoms (the Ni–Ni bridge) and one with Al atoms (the Al–Al bridge). Finally, there are two on-top sites, one for each element in the surface.

The three adsorbates we investigate here are very different in size. The smallest adsorbate is sulfur, with an atomic radius of 1.025 Å, smaller than both Ni and Al (1.246 Å and 1.432 Å, respectively). In view of the behavior of small atoms on bcc(1 1 0) surfaces, we might expect S to show a preference for adsorbing in one of the threefold sites on NiAl(1 1 0), although since the even smaller atom C (atomic radius of 0.713 Å) adsorbs on the long-bridge site on Fe(1 1 0) [58], S may adsorb at that site instead. Platinum has an atomic radius of 1.388 Å, which makes it larger than Ni but smaller than Al, large enough to perhaps prefer a long-bridge (pseudo-fourfold) site. The largest adsorbate in this work is Hf. Its radius of 1.564 Å makes it larger than both Ni and Al, suggesting that it could also adsorb in a long-bridge site. As we shall see, the metal adsorbates instead prefer to restructure the surface to optimize their interactions.

Adsorption site preferences may correlate not only with size but with the electronegativity of the adatoms, i.e., with how strongly an atom will attract electrons from the surrounding atoms. Sulfur has the largest electronegativity, followed by Pt, Ni, Al, and finally Hf, which has the lowest electronegativity. We shall see below how these electronegativity differences contribute to the adsorption behavior.

4.1. Adsorption of S on NiAl(1 1 0)

Table 3 displays the predicted adsorption energies for sulfur on NiAl(1 1 0), as well as the nature of the critical points derived from the analysis of the eigenmode frequencies for each site, which are presented in Table 4. The two threefold sites, 2Ni–Al and Ni–2Al, are the only stable minima. Of these two sites, the 2Ni–Al is the most stable, with the Ni–2Al site 0.22 eV higher in energy. Of the three possible bridge sites on NiAl(1 1 0), we find that adsorption of S in the Ni–Al short-bridge site is unstable, with S relaxing to the energetically most favorable 2Ni–Al threefold minimum. The two long-bridge sites, Ni–Ni and Al–Al, are predicted to be transition states, where the imaginary frequencies in each case are coupled to the motion along the line connecting the closest threefold site with the long-bridge site (see Table 4). Thus, the long-bridge sites

Table 3
PAW-DFT-GGA(PBE) adsorption energies, in eV, for the adsorption of 0.125 ML S, Pt, and Hf on NiAl(1 1 0)

Site	$E_{ads,S}$	Type of state	$E_{ads,Pt}$	Type of state	$E_{ads,Hf}$	Type of state
Al on-top	−3.21	HOSP	−4.03	HOSP	−3.70 [−3.64]	HOSP
Ni on-top	−3.50	HOSP	−4.30	HOSP	−4.42 [−4.36]	"TS"
Ni–Al bridge	→ 2Ni–Al (min)		→ Ni–2Al ("TS")		→ Ni–Ni bridge (min)	
Al–Al bridge	−4.53	TS	−5.29	"TS"	**−4.22** [−4.14]	**Min**
Ni–Ni bridge	−4.91	TS	**−5.30**	**Min**	**−5.00** [−4.91]	**Min**
Ni–2Al, threefold	**−4.69**	**Min**	−5.27	"TS"	→ Ni, on-top ("TS")	
2Ni–Al, threefold	**−4.91**	**Min**	→ Ni–Ni bridge (min)		→ Ni–Ni bridge (min)	

Min = minimum, TS = transition state, and HOSP = higher order saddle point. The "TS" label is used for sites with one imaginary frequency, where the magnitude of this frequency is less than 50 cm^{-1} (see Table 4). Arrows indicate that the high-symmetry initial guess relaxed to a different (indicated) geometry. Energies for minima are shown in boldface. Numbers in square brackets for Hf are results after correction for the spurious energy due to interactions of the surface dipole moment with its periodic images.

Table 4
Frequencies, in cm^{-1}, of the three eigenmodes of the adatoms in the six metastable sites

Site	S adatom		Pt adatom		Hf adatom	
	Normal	Frustrated	Normal	Frustrated	Normal	Frustrated
Al on-top	523, 134	151i, 167i	80	62i, 70i	118	22i, 33i
Ni on-top	390, 134	169i, 198i	90	58i, 76i	93	37, 29i
Al–Al bridge	470	146, 143i	83	47, 32i	72	44, 21
Ni–Ni bridge	351	109, 100i	74	46, 29	75	52, 35
Ni–2Al, threefold	427	105, 40	76	37, 30i	→ Ni, on-top ("TS")	
2Ni–Al, threefold	272	101, 29	→Ni–Ni bridge (min)		→ Ni–Ni bridge (min)	

The "normal" modes are the vibrations along the surface normal, while the "frustrated" (translation) modes have eigenvectors parallel to the surface. It is impossible to extract an eigenmode for sulfur that is dominated by the adatom for the on-top sites due to strong adsorbate-surface coupling. The larger of the two numbers refers to the out-of-phase mode between the adatom and the on-top substrate atom, a mode that changes the distance between the two atoms, and the smaller frequency is for the in-phase mode where the distance between the adatom and on-top substrate atom is more or less constant.

are predicted to be transition states for diffusion between neighboring threefold sites. However, we predict essentially no barrier (less than 0.01 eV) between the 2Ni–Al threefold minimum and the corresponding Ni–Ni "transition state", suggesting that S can freely move between neighboring 2Ni–Al sites. For the other minimum-transition state couple, Ni–2Al and Al–Al, we predict a small barrier of 0.16 eV. Lastly, the two on-top adsorption sites are predicted to be higher order saddle points, with two imaginary frequencies coupled to motion parallel to the surface (see Table 4).

The local surface rippling upon adsorption of sulfur is displayed in Table 5. For the two threefold site minima, the rippling is about the same as for the clean surface, with Al atoms roughly 0.2 Å higher than the Ni atoms. In this way, the Al atoms create a ridge surrounding a trough of Ni atoms. The homonuclear Ni–Ni and Al–Al bridge sites are transition states for S diffusion. As the S diffuses from the threefold minima to the twofold transition states, we predict quite different local structural responses to the diffusion. The sulfur atom induces a somewhat deeper Ni trough of 0.24 Å at the Ni–Ni bridge transition state. By contrast, sulfur flattens out the rippling locally in the Al–Al bridge transition state.

Table 5
Height differences, Δd_{11}, in Å between surface Al and Ni atoms closest to the adsorbed atom

System	S adatom	Pt adatom	Hf adatom
Al on-top	−0.02	−0.38	−0.83
Ni on-top	+0.37	+0.77	+0.55
Ni–Al bridge	→ 2Ni–Al	→ Ni–2Al	→ Ni–Ni bridge
Al–Al bridge	+0.015	−0.002	−0.40
Ni–Ni bridge	+0.24	+0.31	+0.02
Ni–2Al, threefold	+0.17	+0.13	→ Ni, on-top
2Ni–Al, threefold	+0.20	→ Ni–Ni bridge	→ Ni–Ni bridge

Recall that the clean surface rippling $\Delta d_{11} = 0.17$ Å. When Al is above Ni, as in the clean surface, the value is positive; when Ni is above Al, the value is negative.

Table 6 displays additional information about adsorbate-induced surface structural changes, in the form of distances to nearest (NN) and next-nearest (NNN) neighbors to the adsorbate. The S–Ni distances are consistently shorter than S-Al distances, suggesting a somewhat stronger interaction between S and Ni than between S and Al. This is consistent with the binding energies of Table 3, where the 2Ni–Al threefold site is found to be the lowest energy site. Moreover, we see that only in the two threefold site minima are both the NN and the NNN distances less than the sum of the atomic radii, indicating strong bonding. In all other sites, only NN distances fall in this bonding range. The nearest neighbor distances to Ni and to Al are almost identical in the diffusion transition states (i.e., the two bridge sites). The transition states differ strongly only at second nearest neighbors: here the S–Al distance in the Ni–Ni bridge transition state is significantly shorter than

Table 6
Distances (Å) between the adsorbate and its nearest (NN) and next-nearest (NNN) neighbors

System	S adatom		Pt adatom		Hf adatom	
	r_{NN}	r_{NNN}	r_{NN}	r_{NNN}	r_{NN}	r_{NNN}
Al on-top	2.14(Al, 88%)	3.32(Ni, 146%)	2.21(Al, 79%)	3.09(Ni, 117%)	2.44(Al, 82%)	2.84(Ni, 101%)
Ni on-top	2.10(Ni, 93%)	3.06(Al, 125%)	2.31(Ni, 88%)	2.87(Al, 102%)	2.17(Ni, 77%)	3.01(Al, 100%)
Ni–Al bridge	→ 2Ni–Al, threefold		→ Ni–2Al, threefold		→ Ni–Ni bridge	
Al–Al bridge	2.27(Al, 93%)	2.64(Ni, 116%)	2.34(Al, 83%)	2.71(Ni, 103%)	2.56(Ni, 91%)	2.63(Al, 88%)
Ni–Ni bridge	2.26(Ni, 99%)	2.49(Al, 102%)	2.46(Ni, 93%)	2.52(Al, 90%)	2.35(Ni, 84%)	2.80(Al, 94%)
Ni–2Al, threefold	2.26(Ni, 99%)	2.32(Al, 95%)	2.37(Al, 84%)	2.52(Ni, 94%)	→ Ni, on-top	
2Ni–Al, threefold	2.26(Ni, 99%)	2.30(Al, 94%)	→ Ni–Ni bridge		→ Ni–Ni bridge	

The type of atom that is the NN or NNN for each site and the corresponding percentage of the sum of the atomic radii for the adatom-neighbor pair are given in parentheses.

the S–Ni distance in the Al–Al bridge transition state. The effectively higher coordination of S in the Ni–Ni bridge transition state may explain its lower energy. Also, the geometry of the preferred adsorption site is not very different from the geometry of the Ni–Ni bridge site, and the energy difference between these sites is negligible in our calculations. The preferred threefold site can be seen as adsorption in a position slightly off the Ni–Ni bridge site. Since there is very little difference between the 2Ni–Al threefold minimum site and Ni–Ni bridge transition state in structure, it is not surprising that there is no difference in energy between these sites in our calculation. On the other hand, there is a significant energy difference between the Ni–2Al threefold minimum site and the Al–Al bridge transition state. Here we find a larger difference in geometry between the sites, in particular the Ni–S bond length is increased almost 0.4 Å when the S adatom is moved from the Ni–2Al threefold to the Al–Al bridge site. This increased Ni–S distance, and the local flattening of the surface for the Al–Al bridge transition state, contributes to the larger energy difference between this minimum-transition state pair.

Inspection of the changes in electron density upon S adsorption on the NiAl(1 1 0) surface (see Figs. 2 and 3) shows that charge accumulates between the S adatom and the Ni and Al substrate atoms. The accumulation of electron density is larger between S–Al than between S–Ni for both threefold site minima. This can be understood in terms of electronegativity, where S is the most and Al the least electronegative of the three elements involved. Thus, electrons localize between the elements with the largest electronegativity difference, creating polar covalent bonds. The structure in $\Delta\rho$ seen is due to the interaction between the p-states of S and d-states of Ni, i.e., the dumbbell-shaped depletion of density around the Ni atoms is due to d-states being emptied. This conclusion is supported by the LDOS in Fig. 5, where we present the LDOS for the adsorbates and the Ni substrate atoms for the most stable adsorption site for each adsorbate. The LDOS for Al substrate atoms are an order of magnitude smaller than the Ni LDOS, due to the delocalization of the sp-electrons on Al, and therefore less informative (and are not shown). The LDOS for sulfur show that its atomic states are broadened and their energies decrease upon adsorption. This is due to interaction with Ni d-states, which are clearly perturbed by the adsorbate, as seen by comparing the top left and bottom left panels in Fig. 5.

4.2. Adsorption of Pt on NiAl(1 1 0)

The adsorption energies for Pt on NiAl(1 1 0) are displayed in Table 3 along with the analysis of the eigenfrequencies for the vibrational modes of the adsorbate. We find only one unambiguous minimum: the Ni–Ni bridge site. Two other sites are very similar in stability but both possess an imaginary frequency of small magnitude (see Table 4), suggesting they may not be true minima. These two sites, the Ni–2Al threefold site and the Al–Al bridge site, are thus designated as "TS" for "possible transition state". Initial adsorption of Pt in the other threefold site, 2Ni–Al, is unstable with respect to the Pt atom moving to the Ni–Ni bridge minimum. As in sulfur adsorption, the mixed Ni–Al bridge adsorption site is unstable with respect to motion of the Pt atom to a threefold site, in this case Ni–2Al. The on-top sites are higher energy, higher order saddle points, as expected.

Table 5 displays the local surface rippling induced by the Pt adsorbate. The changes in surface structure due to metal atom adsorption at all sites, even unstable saddle points, may help us gain insight into the dynamics of metal atom deposition in thin film growth, since under such conditions all sites are equally likely to be accessed, at least momentarily. For the Ni–Ni bridge site minimum, the local rippling is considerably enhanced compared with the clean surface. For the threefold Ni–2Al "TS", the local rippling is suppressed slightly, while the Al–Al bridge "TS" exhibits a flat local geometry with no rippling. The local geometry for the on-top higher-order saddle point sites exhibit even larger changes, with Al 0.77 Å above Ni when Pt adsorbs on-top of Ni (i.e., the Ni substrate atom is pushed 0.6 Å deeper into the bulk compared to the clean surface) and with Al pushed deeper into the surface by 0.55 Å compared to the clean surface when Pt is adsorbed on top of Al. The rippling pattern is completely reversed in sign for Pt adsorbed on Al. Of course, any Pt atom adsorbing on either HOSP will not stay there long, so any adsorbate-induced rippling effect there will be altered as soon as Pt moves to the Ni–Ni

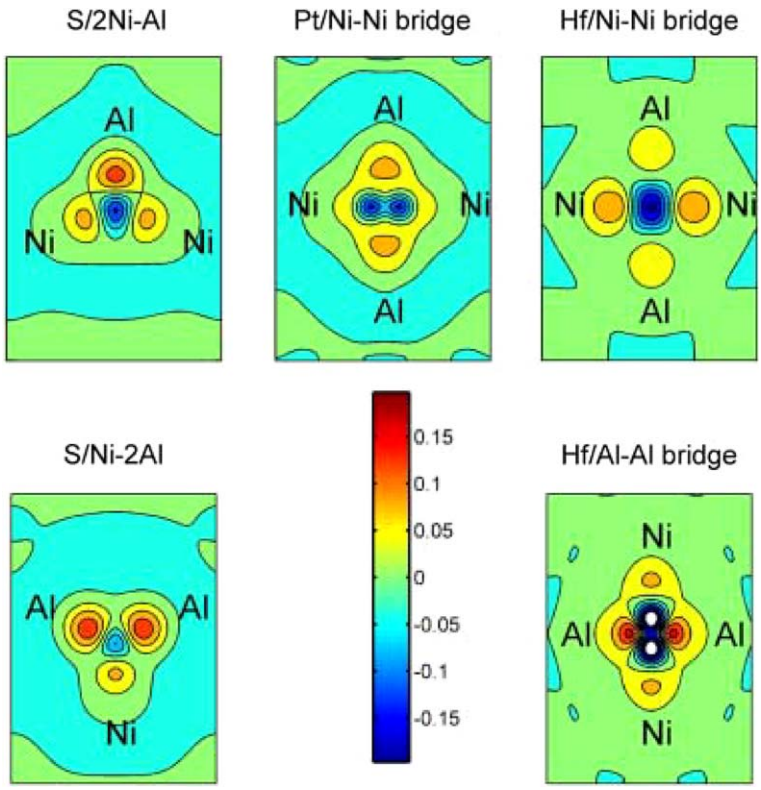

Fig. 2. Electron density differences as cuts through planes parallel to the surface midway between the adsorbate and surface layer. The panels to the left show S adsorption, middle panel shows Pt, and right panels show Hf. Top row shows the Ni-dominated adsorption sites and the bottom row shows the Al-dominated ones. Accumulation of electron density is shown in red–yellow and depletion in blue, see legend (density difference given in $Å^{-3}$). (For interpretation of the references in colour in this figure legend, the reader is referred to the web version of this article.)

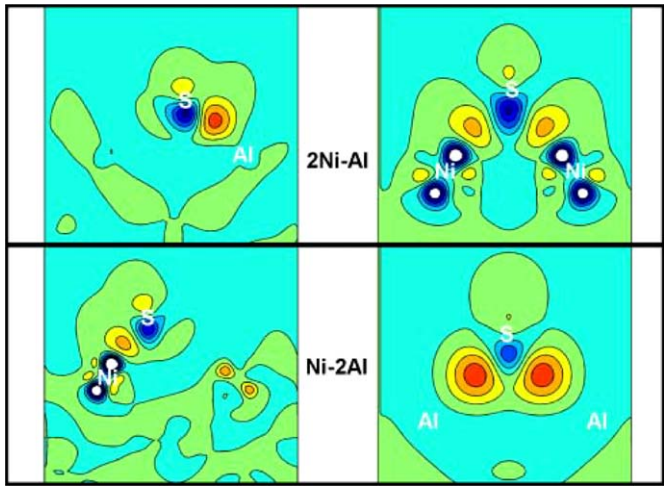

Fig. 3. Electron density differences as cuts through planes containing S–Ni and S–Al bonds for the S adatom on the 2Ni–Al (top) and Ni–2Al (bottom) threefold sites. Cuts through the adatom and the minority substrate atom on the left and cuts through the adatom and the two majority substrate atoms are on the right. Note that the length scales of the left and right panels are not identical. White text marks the position of the ions. Red–orange shows accumulation and blue depletion of electron density upon adsorption, with the same color scale as the legend in Fig. 2. White areas in plot show areas where the density is decreased more than the color scale. (For interpretation of the references in colour in this figure legend, the reader is referred to the web version of this article.)

bridge site minimum. However, it suggests that surface phonons might be excited by such an initial adsorption event.

Table 6 provides additional information about the local geometry via the distance between the Pt atom and its nearest and next nearest neighbors. The Pt–Al distances are generally shorter than their equivalent Pt–Ni distances. For the Ni–Ni bridge site, the next-nearest-neighbor distance is only 2% longer than the nearest-neighbor distance; hence the effective coordination for the Pt atom is increased from 2 to 4. This increased coordination may explain why the Ni–Ni bridge site is a minimum while the Al–Al bridge and Ni–2Al sites may be transition states. The Ni–2Al has only threefold coordination, while the NNN distance for the Al–Al bridge site is too large to give fourfold coordination.

Electron density difference plots (Figs. 2 and 4) show that electron density accumulates mainly on Pt (red contours of Fig. 4), as well as between Pt and Al. This is consistent with the electronegativity of the three elements which is largest for Pt, and charge localizes between pairs of elements with the largest electronegativity difference (here Pt and Al). The localization is less than for S, since Pt is less electronegative, yielding a less polar bond. The largest changes in the electron density occur around Ni and Pt, where the d-orbitals are interacting, giving lots of

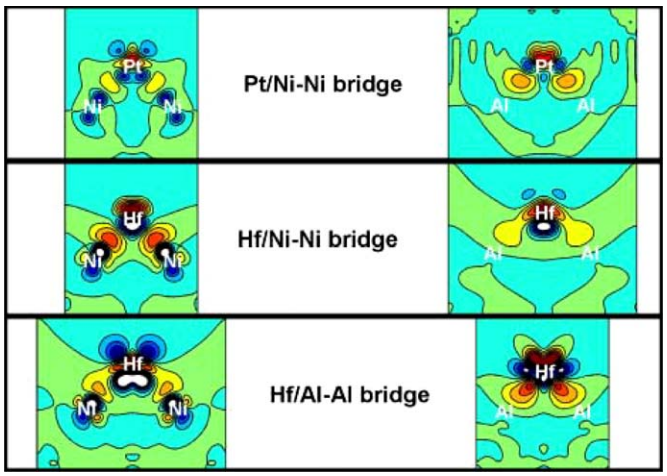

Fig. 4. Electron density differences as cuts through planes perpendicular to the surface for metal adatoms. Cuts through the adatom and Ni atoms from the substrate are on the left, and cuts through the adatom-Al substrate atoms are on the right. White text marks the position of the ions. The top panel shows Pt adsorbed in the Ni–Ni bridge site, the middle panel shows Hf in the Ni–Ni bridge site and the bottom panel shows Hf in the Al–Al bridge site. Red–orange shows accumulation and blue depletion of electron density upon adsorption, with the same color scale as the legend in Fig. 2. White areas in plot show areas where the density is decreased more than the color scale. (For interpretation of the references in colour in this figure legend, the reader is referred to the web version of this article.)

structure to the $\Delta\rho$ plots (see Fig. 4). These significant perturbations in the electron density are also seen in changes in the LDOS upon adsorption. The LDOS for the Pt atom changes strongly upon adsorption and the Ni LDOS is also drastically altered upon Pt adsorption (Fig. 5). Not only are the energies of the Pt states lowered and broadened, but they are strongly mixed with Ni d-states, suggesting strong metallic bonding between Ni and Pt at the Ni–Ni bridge site. Thus Pt forms polar metallic bonds to Al and rather covalent metallic bonds to Ni.

4.3. Adsorption of Hf on NiAl(110)

Table 3 also presents adsorption energetics for Hf on NiAl(110). The two single element bridge sites are found to be unambiguous minima, in contrast to Pt where only the Ni–Ni bridge site was a clear minimum. The Ni–Ni bridge site for Hf is the most stable adsite, with the Al–Al bridge site 0.78 eV higher in energy. The Ni on-top site has one small magnitude imaginary frequency (see Table 4); hence we designate this as a "TS", for a possible transition state to the Ni–Ni bridge minimum. To check this, we moved the Hf atom a short distance off the high-symmetry Ni on-top site and showed that ionic relaxation moves the Hf to the Ni–Ni bridge site minimum. Thus, it may be that Hf atoms diffuse one-dimensionally, with a barrier of 0.6 eV, along the Ni rows on the surface. The Al on-top site is predicted once again to be a higher order saddle point, just as in the S and Pt adsorbate cases. The three other possible high-symmetry sites are all unstable,

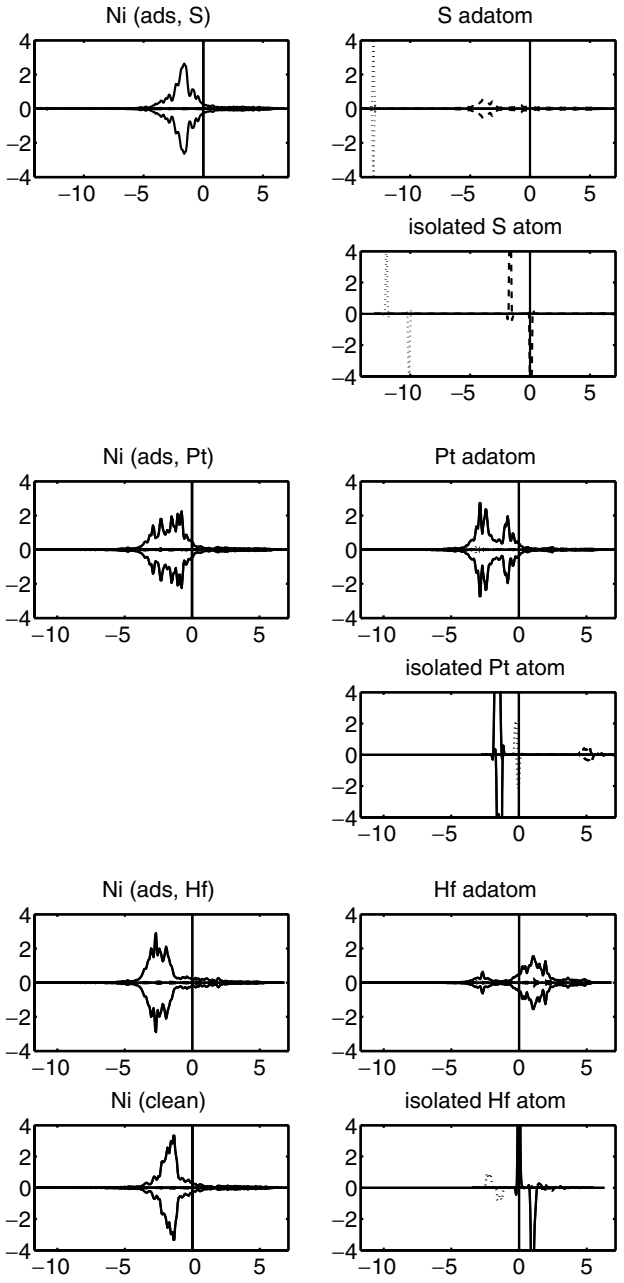

Fig. 5. Projected local density of states (LDOS) for S, Pt, and Hf adatoms, and Ni substrate atoms before and after adsorption. The Al LDOS is negligible and is not shown. Dotted lines are s-states, dashed lines are p-states, and solid lines are d-states. Spin-up states are shown with positive values and spin-down states are shown with negative values. The panels on the left side show the Ni atoms from the substrate, and the panels on the right side show the adatoms. The first row shows S at the 2Ni–Al threefold site, the second row shows an isolated S atom, the third row shows Pt at the Ni–Ni bridge site, the fourth row shows an isolated Pt atom, the fifth row shows Hf at the Ni–Ni bridge site, and the last row shows a Ni atom from the clean NiAl(110) to the right and an isolated Hf atom to the left.

with ionic relaxation moving the Hf atom from the initial guesses for these sites to other sites. The Ni–2Al threefold initial guess moves the Hf to the Ni on-top site, while the 2Ni–Al threefold and Ni–Al mixed bridge sites both move the Hf to the Ni–Ni bridge minimum.

We also analyzed the adsorbate-induced local rippling for Hf adsorption; the results are shown in Table 5. The Ni–Ni bridge minimum has a locally flat geometry, in contrast to the S and Pt adsorption geometries at this site. Hf is 0.35 Å and 1.08 Å larger in diameter than Pt and S, respectively. The flat surface geometry apparently suppresses interaction with nearby Al atoms. By contrast, the Al–Al minimum exhibits a reversed rippling upon Hf adsorption: the nearest neighbor Al atoms are 0.40 Å below the nearest Ni atoms. Given the preference for Al to be at the surface, this may explain why this Al–Al bridge site is less stable than the Ni–Ni bridge. The change in local rippling is even larger for the on-top sites. As with the Pt adsorbate, the atoms under the Hf are pushed down, dramatically changing the local rippling. The adsorption and diffusion of Hf on the NiAl(1 1 0) surface is likely to be connected to excitation of surface phonons, as suggested for Pt adsorption.

Additional structural information about the Hf adsorption sites can be found in Table 6, where we present the distances between Hf and its nearest and next-nearest neighbors. The Hf–Ni NN distance is significantly shorter than the Hf–Al NN distance in all cases. While the Ni atoms are nearest neighbors to Hf in the Ni–Ni bridge minimum as expected, large structural rearrangements occur in the Al–Al bridge site minimum. In particular, the two initially next-nearest-neighbor Ni atoms decrease their distance to the Hf atom during ionic relaxation, with the final result that these Ni atoms become Hf's nearest neighbors, while the two Al atoms are next-nearest neighbors! The large structural relaxations for the Al–Al bridge site give this site a Ni–Ni bridge appearance; the residual strain in the final structure might explain the energy difference between the two homonuclear bridge sites. For the Ni on-top transition state, the Hf–Ni distance is 2.17 Å, much shorter than the corresponding nearest-neighbor distance for the Al on-top site (2.44 Å), once again suggesting stronger Hf–Ni interactions than Hf–Al interactions.

Hf has a lower electronegativity than Ni and Al, in contrast to the other adsorbates considered here, with the largest difference in electronegativity between Hf and Ni. Thus, we might expect that Hf will donate charge to the substrate atoms, in particular to the Ni atoms. What we find instead is a more complex interaction between the adatom and the substrate atoms. From the electron density differences in Fig. 2 it is clear from the cut parallel to the surface that more electron density accumulates between Hf and Ni for the Ni–Ni bridge site, while the largest increase is between Hf and Al atoms for the Al–Al bridge site. From the cuts perpendicular to the surface (Fig. 4), we see very dramatic changes in the density around Hf and Ni, with negligible change around the Al atoms. The Hf atom is clearly rehybridizing, polarizing its electron density to form strong polar bonds with the metal substrate. It appears that Ni also repolarizes to put more electron density between the Hf and Ni, as opposed to remaining centered on the Ni atom. The LDOS plot (Fig. 5) shows that the partially occupied d-states on Hf in the gas phase are indeed mostly emptied upon adsorption, consistent with a transfer of charge to the substrate atoms. We see a corresponding shift in the Ni d-states to lower binding energies and filling of more d-states below the Fermi level, corresponding to charge transfer from Hf to Ni.

5. Discussion and conclusions

In this work, we have investigated the adsorption of S, Pt, and Hf atoms on NiAl(1 1 0), in order to characterize the interactions of S impurities and Pt and Hf dopants present at the surface of NiAl alloy bond coats. We find that S prefers to adsorb in a threefold hollow site containing two Ni and one Al atom, whereas Pt and Hf favor adsorption in Ni–Ni bridge sites. The latter finding is consistent with STM data for a variety of metals (Pd, Au, Mn, Fe, and Co) [40,41], suggesting that it is a general trend for all metal adsorption on NiAl(1 1 0). That S prefers to bind to Ni-dominated threefold hollow sites is consistent with how S adsorbs on Ni(1 1 1) [61,62] and how H adsorbs on NiAl(1 1 0) [1,29,28]. We predict that Pt adsorbs more strongly to the NiAl surface (by 0.3–0.4 eV) than either of the other two adsorbates, while Hf is only slightly more strongly bound than S. Interestingly, both metal adatoms are predicted to induce significant local restructuring of the originally-rippled bare surface, while S exhibits no such dramatic structural changes. This local restructuring might induce surface phonon excitation. We also find that S can diffuse easily between threefold sites and that Hf has a reasonably low (0.6 eV) barrier to diffusion along the Ni rows. Other low-symmetry diffusion transition states may exist, but we did not find them during our search.

As alluded to above, S adsorption on NiAl(1 1 0) has features similar to predictions for adsorption of H on NiAl(1 1 0). H was predicted to adsorb slightly off the Ni–Ni bridge site [1,29], and vibrational frequency analysis showed this is a true minimum [29]. LEED and surface extended X-ray fine structure (SEXAFS) data indicate that S adsorbs in threefold hollow sites on Ni(1 1 1) [61,62], consistent with our findings here. Open-shell atoms tend to prefer higher coordination sites.

The adsorbate-induced restructuring achieved by Pt manifests itself by bringing NNN Al atoms close to the NN Ni atoms in the Ni–Ni bridge such that the Pt is effectively fourfold coordinated. This affinity that Pt appears to have for Al also shows up in the shorter bond lengths (compared to Pt–Ni) and greater charge localization between Pt and Al than between Pt and Ni. The more electropositive Al donates charge to the more electronegative Pt to create polar metallic bonds, while Pt and Ni interact via covalent metallic bonds.

The adsorbate-induced restructuring due to Hf adsorption is different than that for Pt: Hf suppresses the rippling. Also, based on an analysis of bond lengths, and the fact that the Al–Al bridge actually rearranges to bring Ni atoms into nearest neighbor positions(!), Hf appears to have a

higher affinity for Ni than for Al, which is the opposite of Pt's interaction. The flattening of the surface upon Hf adsorption can also be understood as a means to keep Al further away from the adsorbate. Hf adsorption produces significant charge rearrangement in order to create strong metal-metal bonds between Hf and Ni, while Al remains less perturbed.

We can also attempt to understand these findings in terms of trends in thermodynamic properties. For example, the energies of formation of Hf–Ni alloys are more negative (more stable) than Hf–Al alloys [63], consistent with our findings that Hf appears to have a greater affinity for Ni than for Al. Pt is infinitely soluble in Ni, but the only formation energy tabulated for a Ni–Pt alloy is quite small [63]. By contrast, Pt is nearly completely insoluble in Al and forms a variety of intermetallic compounds, all of which have quite negative formation energies (indicating their high stability). This also is consistent with our findings that Pt appears to have a higher affinity for Al than for Ni.

Thus, we have elucidated some of the differences between S impurities and Pt and Hf dopants on NiAl surfaces. While the tendency for the metal atoms to adsorb in Ni–Ni bridge sites has already been observed with STM, our other findings await experimental verification. We end with minor speculations as to how these predictions may prove relevant for understanding materials interfaces. Sulfur's weaker binding and ease of diffusion may also hint at its role in apparently weakening adhesion between metals and their corresponding oxide scales. Pt's and Hf's stronger interactions with the NiAl substrate may point to their roles in stabilizing that same metal–oxide scale interface. Our ongoing research aims to test such ideas.

Acknowledgement

We are grateful to the Air Force Office of Scientific Research (AFOSR) for funding of personnel and computing time at the Maui High Performance Computing Center (MHPCC).

References

[1] A.T. Hanbicki, A.P. Baddorf, E.W. Plummer, B. Hammer, M. Scheffler, Surf. Sci. 331–333 (1995) 811.
[2] D.B. Miracle, Acta Metall. Mater. 41 (3) (1993) 649.
[3] R. Franchy, Surf. Sci. Rep. 38 (2000) 195.
[4] D. Zhu, R.A. Miller, MRS Bull. (2000) 43.
[5] N.P. Padture, M. Gell, E.H. Jordan, Science 296 (2002) 280.
[6] J.R. Nicholls, JOM 52 (2000) 28.
[7] D.A. Ford, K.P.L. Fullagar, H.K. Bhangu, M.C. Thomas, P.S. Burkholder, P.S. Korkinko, K. Harris, J.B. Wahl, J. Eng. Gas Turbines Power 121 (1999) 138.
[8] F.H. Scott, D.J. de Wet, R. Taylor, MRS Bull. 19 (1994) 46.
[9] G.W. Goward, Surf. Coat. Tech. 108–109 (1998) 73.
[10] P.K. Wright, A.G. Evans, Cur. Opt. Sol. State Mater. Sci. 4 (3) (1999) 255.
[11] P. Villars, L.D. Calvart (Eds.), Pearson's Handbook of Crystallographic Data for Intermetallic Phases, second ed., ASM International, Ohio, USA, 1991.
[12] P. Mrozek, A. Jablonski, Surf. Sci. 208 (1989) 351.
[13] M.H. Yoo, C.L. Fu, Scripta Metall. Mater. 25 (10) (1991) 2345.
[14] H.L. Davis, J.R. Noonan, Phys. Rev. Lett. 54 (6) (1985) 566.
[15] S.M. Yalisove, W.R. Graham, Surf. Sci. 183 (1987) 556.
[16] M.H. Kang, E.J. Mele, Phys. Rev. B 36 (14) (1987) 7371.
[17] E.A.A. Jarvis, R.L. Hayes, E.A. Carter, ChemPhysChem 2 (1) (2001) 55.
[18] E.A.A. Jarvis, A. Christensen, E.A. Carter, Surf. Sci. 487 (2001) 55.
[19] A.V. Ruban, H.L. Skriver, J.K. Nørskov, Phys. Rev. B 59 (24) (1999) 15990.
[20] J.R. Noonan, H.L. Davis, Science 234 (4774) (1986) 310.
[21] D.R. Mullins, S.H. Overby, Surf. Sci. 199 (1988) 141.
[22] S.M. Yalisove, W.R. Graham, J. Vacuum Sci. Tech. A 6 (3) (1988) 588.
[23] S.-C. Lui, M.H. Kan, E.J. Mele, E.W. Plummer, D.M. Zehner, Phys. Rev. B 39 (18) (1989) 13149.
[24] M. Mostoller, R.M. Nicklow, D.M. Zehner, S.-C. Lui, J.M. Mundenar, E.W. Plummer, Phys. Rev. B 40 (5) (1989) 2856.
[25] J.I. Lee, C.L. Fu, A.J. Freeman, Phys. Rev. B 36 (17) (1987) 9318.
[26] B. Hammer, M. Scheffler, Phys. Rev. Lett. 74 (17) (1995) 3487.
[27] A. Hanbicki, H.L. Davis, A.P. Baddorf, D.B. Poker, E.W. Plummer, Surf. Sci. 365 (1996) L639.
[28] D. Farías, M. Patting, K.H. Rieder, J. Chem. Phys. 117 (4) (2002) 1797.
[29] M. Konôpka, I. Ŝtich, K. Terakura, Phys. Rev. B 65 (12) (2002) 125418.
[30] P. Rivière, H.F. Busengo, F. Martí, J. Chem. Phys. 121 (2) (2004) 751.
[31] G.R. Castro, D. Drakova, M.E. Grillo, G. Doyen, J. Chem. Phys. (21) (1996) 9640.
[32] A.Y. Lozovoi, A. Alavi, M.W. Finnis, Phys. Rev. Lett. 85 (3) (2000) 610.
[33] H. Isern, G.R. Castro, Surf. Sci. 211–212 (1989) 865.
[34] J. Jacobsen, B. Hammer, K.W. Jacobsen, J.K. Nørskov, Phys. Rev. B 52 (20) (1995) 14954.
[35] Y. Yourdshahyan, B. Razaznejad, B.I. Lundqvist, Phys. Rev. B 65 (2002) 075416.
[36] A. Eichler, F. Mittendorfer, J. Hafner, Phys. Rev. B 62 (7) (2000) 4744.
[37] S. Yamagishi, S.J. Jenkins, D.A. King, Surf. Sci. 543 (2003) 12.
[38] N. Nilius, T.M. Wallis, W. Ho, J. Chem. Phys. 117 (24) (2002) 10947.
[39] T.M. Wallis, N. Nilius, W. Ho, J. Chem. Phys. 119 (4) (2003) 2296.
[40] N. Nilius, T.M. Wallis, M. Persson, W. Ho, Phys. Rev. Lett. 90 (19) (2003) 196103.
[41] H.J. Lee, W. Ho, Phys. Rev. Lett. 92 (18) (2004) 186802.
[42] B.A. Pint, Oxid. Met. 45 (1–2) (1996) 1.
[43] G. Kresse, J. Hafner, Phys. Rev. B 48 (17) (1993) 13115.
[44] G. Kresse, J. Furthmüller, Phys. Rev. B 54 (16) (1996) 11169.
[45] G. Kresse, J. Furthmüller, Comput. Mater. Sci. 6 (1) (1996) 15.
[46] P. Hohenberg, W. Kohn, Phys. Rev. 136 (3B) (1964) B864.
[47] W. Kohn, L.J. Sham, Phys. Rev. 140 (4A) (1965) A1133.
[48] J.P. Perdew, K. Burke, M. Ernzerhof, Phys. Rev. Lett. 77 (18) (1996) 3865;
erratum: Phys. Rev. Lett. 78 (1997) 1396.
[49] P.E. Blöchl, Phys. Rev. B 50 (24) (1994) 17953.
[50] G. Kresse, J. Joubert, Phys. Rev. B 59 (3) (1999) 1758.
[51] H.J. Monkhorst, J.D. Pack, Phys. Rev. B 13 (12) (1976) 5188.
[52] C. Kittel, Introduction to Solid State Physics, seventh ed., Wiley, New York, 1996.
[53] E.A.A. Jarvis, E.A. Carter, J. Phys. Chem. B 106 (2002) 7995.
[54] Y. Mishin, M.J. Mehl, D.A. Papaconstantopoulos, Phys. Rev. B 65 (22) (2002) 224114.
[55] C. Thuault-Cytermann, M.C. Desjonquères, D. Spanjaard, J. Phys. C: Solid State Phys. 16 (1983) 5689.
[56] M. Arnold, G. Hupfauer, P. Bayer, L. Hammer, K. Heinz, B. Kohler, M. Scheffler, Surf. Sci. 382 (1997) 288.
[57] D.E. Jiang, E.A. Carter, Surf. Sci. 547 (2003) 85.
[58] D.E. Jiang, E.A. Carter, Phys. Rev. B 71 (4) (2005) 045402.
[59] J. Toofan, G.R. Tinseth, P.R. Watson, J. Vac. Sci. Technol. A 12 (4) (1994) 2246.

[60] M.J.S. Spencer, A. Hung, I.K. Snook, I. Yarovsky, Surf. Sci. 540 (2003) 420.
[61] D.R. Warburton, P.L. Wincott, G. Thornton, Surf. Sci. 211–212 (1) (1989) 71.
[62] Y.-S. Ku, S.H. Overbury, Surf. Sci. 276 (1–3) (1992) 262.
[63] F.R. de Boer, R. Boom, W.C.M. Mattens, A.R. Miedema, A.K. Niessen (Eds.), Cohesion in Metals, vol. 1, North-Holland, 1988.
[64] K. Højrup Hansen, J. Gottschalck, L. Petersen, B. Hammer, E. Lægsgaard, F. Besenbacher, I. Stensgaard, Phys. Rev. B 63 (11) (2001) 115421.